Cylindrical Case Charge (3C) For Artificially Triggering Avalanches Around Mountains, Roads, and Slopes

Dr. Vilem Petr [a], Eduardo Lozano [a], Lea Davis[a], Michael Maestas[a], and Dr. Seetharaman Sridhar[a]

[a] Colorado School of Mines AXPRO Group, 1500 Illinois St., Golden CO, 80401 USA

Abstract

This study overviews a new, advanced avalanche mitigation method using a cylindrical explosive charge placed at the bottom of an avalanche runout zone out-bank of the road shoulder. This research was motivated by the limitation of data on blast wave properties for cylindrical end-initiated charges at high altitude, such as 3,600 to 4,000 m above sea level. These studies characterize a new concept of effectiveness to artificially trigger avalanches from the bottom of the runout zone at the bank of the opposite road shoulder. The current concept to trigger an avalanche is initiating an explosion on the snowpack at the starting zone of the avalanche chute. This new concept uses the advantages of charge size, geometry and slope angle to effectively produce a reflective shockwave with a Mach stem to increase the range of an avalanche mitigation zone. The cylinder side-on shock wave front pressure as a function of the angle and distance from the charge axis were recorded and analyzed. Several parameters were controlled during manufacturing of the cylindrical end-initiated and spherical center-initiation charges including the charge mass, diameter, geometry, density, and external confinement. The large-scale laboratory results and their comparison with the field test results collected by the avalanche mitigation crews of the Colorado Department of Transportation (CDOT) during the 2016/2017 winter season are presented. The experimental data was validated with our experimental model on shock wave interaction on a slope and experimental field data with observations during avalanche mitigation missions by CDOT. The primary objective of the research is to extend this understanding of the new method and explain the new concept on a shock wave reflection from the bottom of the slope

as Mach Stem on snow pack and slope angle.

The CDOT avalanche mitigation crews have replaced the spherical charge with center-initiation and adopted the new cylindrical charge with end-initiated as the new preferred technique in numerous avalanche locations along Rocky Mountains roads, thus confirming that 3C charges are well suited to artificially trigger snow avalanches. In the future, side by side experiments will be needed to analyze the differences of slope topographies and terrain profiles with varying snow depth. Additional quantitative measurements of the blast front pressure (the peak pressure of the leading shock wave) from time-of-arrival measurements during CDOT missions will also need to be taken. This new avalanche mitigation technique is well-suited to mountain roads presenting several advantages over the existing methods: minimum deployment time (road closure), low cost, reduced probability of misfires, simple manufacturing of the charge, and quality control of the charge, flexible and easy to optimize the charge size to specific locations, and reduced operation time in the avalanche danger zone. The research work presented in this paper was done experimental large-scale laboratory experiments and field test results collected by CDOT avalanche mitigation crews during the 2016/2017 winter season.

Keywords: *Case charge, ANFO, avalanche mitigation, blast wave, Mach reflection.*

1. Introduction

Explosives are routinely used to artificially initiate snow avalanches in mountain roads around the West coast of USA as part of efforts to maintain public safety. In the winters of 2009-2017, the Advanced Explosives Processing Research Group (AXPRO) at Colorado School of Mines is helping to the Colorado Department of Transportation (CDOT) research explosive applications for avalanche mitigation. Through this collaboration between CDOT and AXPRO a

new Cylindrical Case Charge (3C) was researched and developed specifically for CDOT applications for high altitude around the roads for avalanche mitigation in the Rocky Mountains region.

Currently the industry is using the term of the "Jug, Bag-Bomb, Sled Bomb, Case Charge, Hand Charge, Turkey Charge, or Helicopter Charge" under this simple definition of case charge: "The detonation of explosive, often multiple bags of Ammonium Nitrate and fuel oil (ANFO), which have been placed (as opposed to thrown or dropped) at the bottom of the targeted avalanche path" (British Columbia Ministry of Transportation). These charges are initiated from the center and usually have spherical shapes. The case charges are placed and initiated at the avalanche fracture zone at the top of the avalanche chute. In the early days of seismic work in Wyoming during 1985-86, large explosive charges of over 35 kg were proved to be a useful tool in mitigating avalanche dangers (L. Livingood 1990).

The new 3C charge is defined as a cylindrical explosive charge, which is characterized by the geometrical diameter/length size ratio of 1/4. The charge geometry is directly related to charge weight. The recommended weights are 10 to 25 kg. The 3C charge is placed on the bottom of the runout zone, typically on the out-bank of the road shoulder. This new method will have the charges at the bottom of the hill rather than the top. Figure 1 shows the key differences between the turkey and 3C charges.

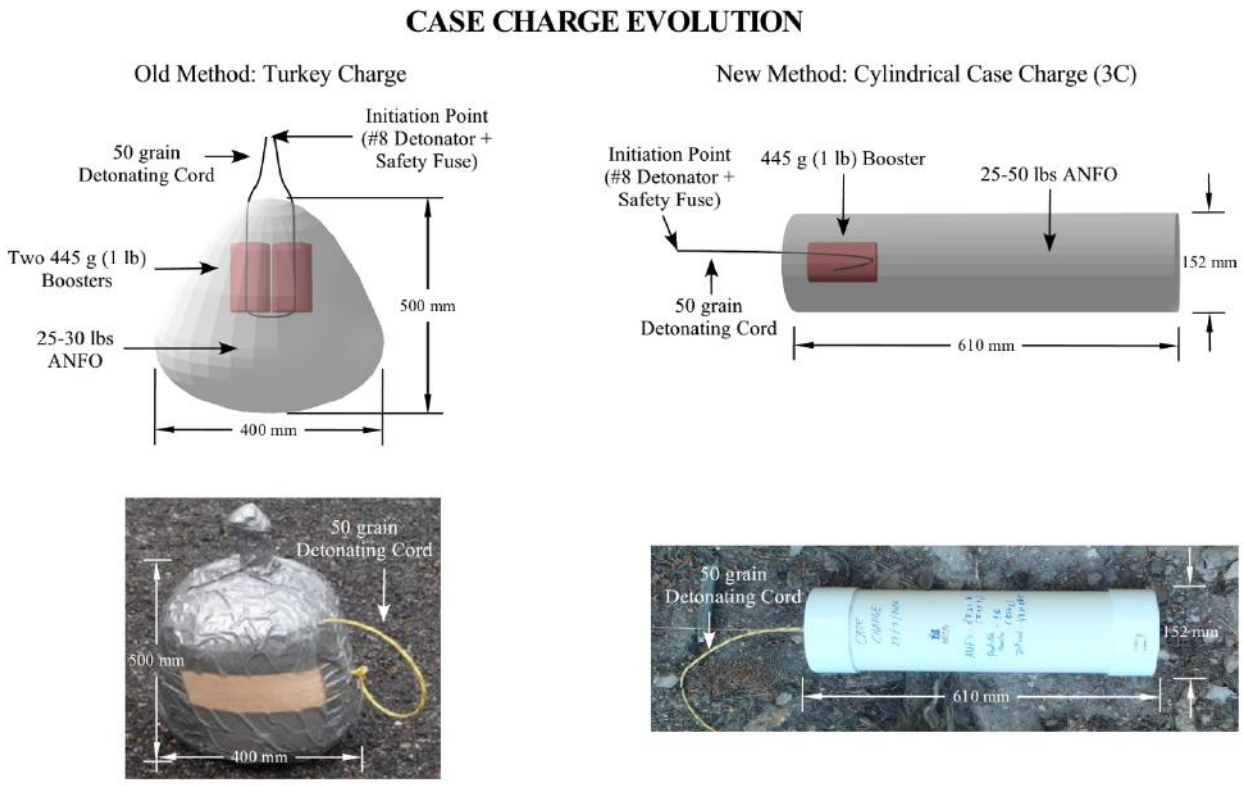

Figure 1. Diagrams and images with key differences between a typical turkey charge (left) and 3C charge (right).

The 3C charge that is approved by the state \and commonly used for avalanche applications is initiated by two standard no. 8 detonators connected to 36 inches of safety fuses (Petr 2016) . The detonators are connected to 600 mm long 50 grain PETN based detonating cord prior to initiation. The detonating cord is then looped through the 450 g Pentolite Booster at a central spot from the one of the ends of the cylinder tube as is shown in Figure 1. Figure 5 shows the 3C charge during assembly. CDOT uses standard schedule 40 PVC for the cylindrical casing. On one end, the PVC is capped for simplicity and filled with bulk explosive materials, generally ANFO. The other end is then also capped to keep the explosive materials in place and initiation system enclosed and protected against moisture during transportation.

The main differences between traditional “case charges or helicopter charges” are in the location of the initiation inside the charges and the cylindrical charge shape as is shown in Figure 1. The expanding shock wave travels up to the avalanche starting zone and produces additional stress on the snow cover creating primary fractures.

During the first winter season 2015/2016, the 3C charge method was implemented, it demonstrated positive results, however some of the technical challenges were not yet resolved. Each avalanche mitigation team used different charge weights, setups, and initiation systems as well inserting the booster in the middle of the PVC tube. The probability of success in inducing an avalanche using 3C charges was based largely on the personnel experience in charge type, size, placement and timing coupled with historical performance of a particular slope. The main goal of this study is to determine the most effective emplacement for avalanche mitigation as well as the best practices to use it in a safe and effective manner. This all depends on the manner in which the shock wave propagates.

1.2 Theory and Background

The sudden energy release from high explosives is accompanied by the creation of a propagating disturbance in the surrounding medium known as shock or blast wave. Detonations in the air produce expanding shock waves that decrease in intensity with distance from the blast due to geometric wave expansion and medium attenuation. Across a shock wave, the air experiences an increase in temperature, density, pressure, and velocity from the front passage. For avalanche mitigation, the pressure jump is the primary loading mechanism into the snowpack. As the primary shock travels over the snow surface, energy is transmitted to the snowpack inducing stress waves within the snow network. Therefore, the effective range of a case charge in triggering

an avalanche will depend directly on the magnitude of the shock wave generated by the explosive and the terrain conditions.

The effective range of a case charge explosive is defined as the distance from the center of the explosion where the additional stress within the snow cover exceeds a threshold value. This threshold value must be sufficiently large to initiate primary shear fracture propagation in a weak point. Although, the peak pressure required for avalanche release is a function of variables such as slope angle or the snow physical parameters, Mellor (1973) suggests loading the anticipated avalanche release zone with at least 3.5 kPa. Following this general criterion, maximizing the effective range then becomes the main goal in this research work. The importance of knowing this effective range is because in most cases avalanches cannot be triggered at every point in the potential release zone. The additional stresses will create fractures of a critical size in the weak points of the snow cover called "hot spots", and from these cracks the avalanche will initiate. It is useful, therefore, to know exactly the effective range of the various sizes of explosive charges. In general, the performance of case charges will depend on the charge physical parameters and location conditions. Such parameters are outlined in Figure 2.

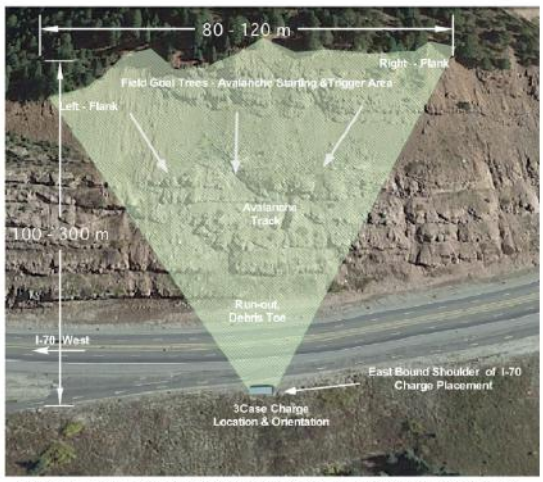

Top view with estimated dimentions of the avalanche mitiagation area

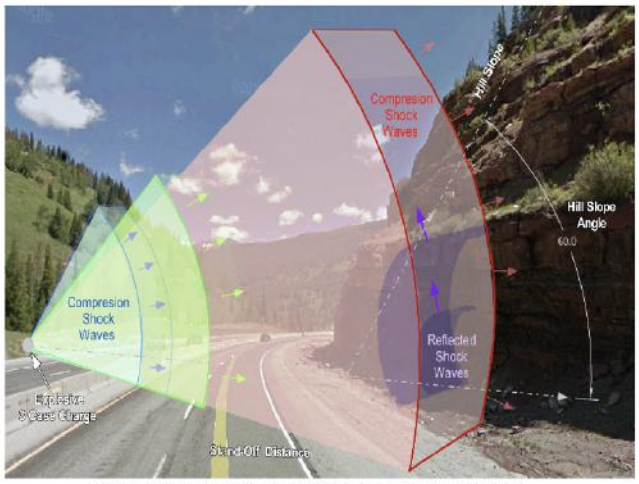

Side view of avalanche mitiagation area using 3C Charge

Figure 2. External location parameters at I-70 Vail pass; top view (left) and side view (right).

1.3 Physical explosive charge parameters

Because of its low cost, high availability, and safe handling, ANFO (ammonium nitrate/fuel oil) was selected as the explosive of choice for comprising the main charge in case charge designs. Alternative explosive materials such as emulsions may also serve as a viable option. Several parameters influence the final performance and energy output from highly non-ideal explosives such as ANFO, e.g., charge mass, diameter, geometry, density, external confinement, etc.

The total mass of explosives influences the effective range that can be created by an explosive charge. In general, larger charges will have a larger effective range. Assuming a spherically expanding shock, this effective range will be proportional to the cubic root of the mass of explosives. For example, in order to double the effective range for a particular charge, eight times the mass of explosives will need to be added. Therefore, the amount of explosives is a critical parameter in order to generate a particular stress on the snow cover, but increasing explosive weight alone is not the most viable of efficient way to increase charge effectiveness. Additionally, the amount of energy released by an explosive charge is a function of the performance of the detonation. One way that the performance of an explosive is quantified, and ultimately the one used in this paper, is by its detonation velocity.

A spherical charge in air will produce a spherical shock wave that expands outward, but for a non-spherical charge, the shock wave will not enter the surrounding air as a spherical wave, nor at the same instant over the entire charge surface. The shape and strength distribution of the shock wave will depend upon both charge geometry and the relative location at which the initiation

occurred. For a cylindrical charge in particular, a maximum output is expected at 90° from the charge axis. Esparza (1992) conducted several studies for the estimation of the equivalency between spherical and cylindrical charges with different length-diameter ratios. For each cylindrical side-on pressure or impulse data point, an equivalent spherical weight was determined that would produce the same side-on pressure or impulse at the same distance. Esparza (1992) reported that a cylindrical charge with a length to diameter ratio of 4 could have and equivalent spherical mass up to three times higher at 90° from the charge axis. That is, 1 kg of a cylindrical HE charge would induce the same blast parameters at 1 m away than 3 kg of the same explosive with a spherical shape. However, experiments show that as one moves radially outward from the detonation center, the shock wave will tend, at some sufficiently large distance, toward a perfect spherical shape and therefore nullify the shape of the charge. Therefore, at longer ranges the cylindrical charge and the spherical charge of the same weight will have pressure peaks that converge to the same value, which will be shown by the tests done in this study.

The charge diameter also plays a major role especially with non-ideal explosives. The detonation velocity will increase asymptotically as we increase charge diameter towards a maximum value called ideal detonation velocity, where maximum performance is achieved (Cooper 1996). This relationship is due to energy loses to the side of the column; when the diameter is large, the losses are small relative to the energy production at the detonation front. With a small diameter, the energy losses are large enough that the velocity of detonation decreases. If the diameter is small enough, energy losses are so great that the chemical reaction causing the detonation will fail propagate at all. At this point, it either slows down to below the sound of speed or stops all together (Cooper 1996). This point is called the critical diameter and for ANFO it can be larger than 100 mm depending on the inert confinement used.

The critical parameters for the detonation/confinement behavior are the thickness of the inert relative to the ZND length, and the difference in detonation to the sound speed (Short et al. 2010). Energy transferred into the confiner from the detonating high explosive can propagate upstream of the detonation shock, driving the confiner into the unreacted explosive, and influencing the detonation performance. For granular non-ideal explosives such as ANFO, the collapse of the pores upstream of the detonation front may lead to local failure of the detonation due to absence of hot-spots, or even early fracture of the confinement (Peter 1983).

Taking into consideration these factors imposes several conditions on the final case charge design. The charges are proposed to have an external cylindrical shape with a minimum length/diameter (L/D) ration of ¼ in this case a length of 610 mm and a diameter of 152 mm, and 0.5 mm thick Polyvinylchloride (PVC) as inert confiner material. The charges must be initiated by one side and primed with at least 454 g booster depending on the charge size.

1.4 Shockwave Reflection Phenomenon

When the incident blast waves from an explosion in air strike a denser medium such as the earth's surface, it is reflected. This reflection can be intentionally created by either detonating the explosive at a certain distance off of the earth's surface or detonating the explosive next to an inclined reflective surface, such as a hill. When this happens, the shock wave will be reflected off of the ground and a second shock wave will be generated behind the first. However, the second wave is traveling through air that has already been heated and compressed by the first wave and as a result, it moves faster than the first wave. Under the adequate conditions, the second wave will eventually overtake the first wave and the two wave fronts merge to form a single front. This phenomenon of wave interaction is called Mach reflection and the final combined shock front is

known as the Mach stem (Figure 3). Any object located in the path of the Mach stem will experience a single shock several times higher than the peak overpressure of the original shock wave. In Figure 3, the blue dotted lines represent the incident shockwave, which is generated by the explosion. The red dotted lines are then the reflected shockwaves off the angled surface. The shock waves are expanding as a function of time and therefore at a certain time the two waves will interact with one another creating the Mach stem shown as the triple point line.

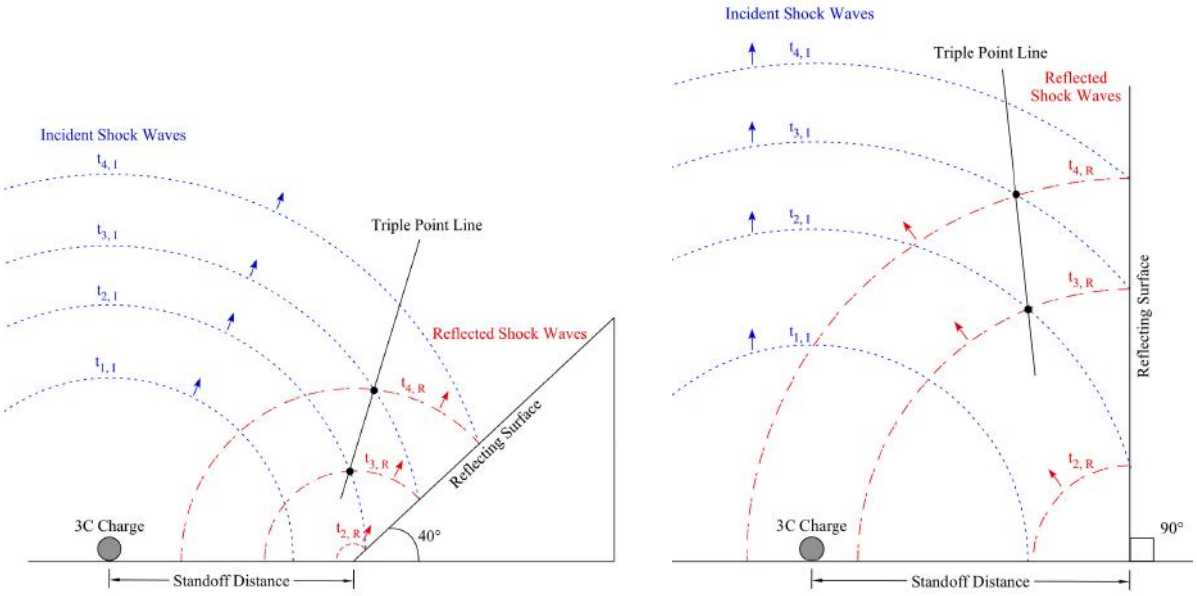

Figure 3. Diagrams of shock wave interactions with a reflecting surface at 40° slope (left) and 90° slope (right).

Depending on the angle of the slope and the strength of the incident shock wave, the type of reflection may be: regular, transitional, double Mach, or single Mach reflection. For steep slopes, usually more than 50°, the transition to from regular to Mach reflection will occur further up the hill. This is because the angle of incidence between the shock and the surface is controlled

by the slope angle (Figure 4). Shadowgraph tests with shock tube were conducted to evaluate the change in reflective shock wave formation depending on slope angle. Shock tube is not strong enough to produce Mach stem pressures in this small-scale experiment, however the presence of reflecting shock waves demonstrates the effects of slope angle. The 90° and 40° slope angle tests both exhibited reflective shock waves, however at 30° there is no evidence of a reflection.

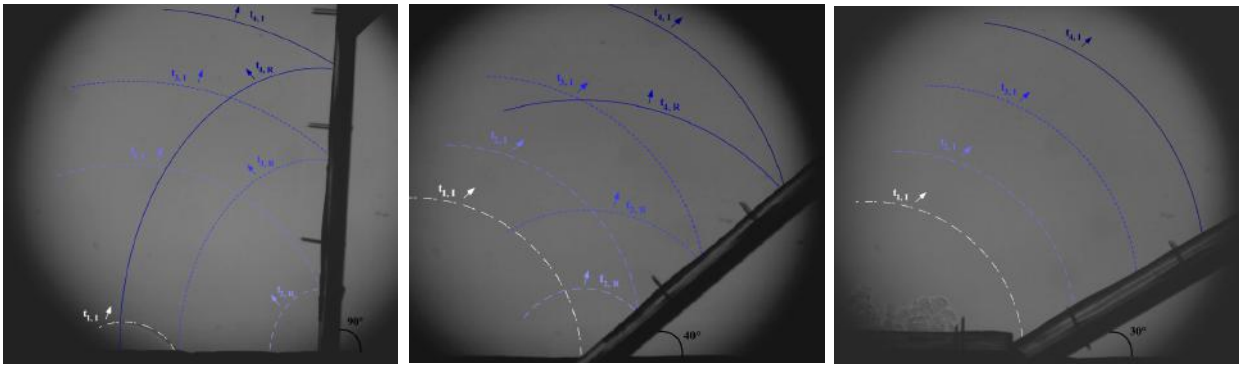

Figure 4. Images of shadowgraph reflection for a 90° angle (left), 40° angle (middle) and 30° angle (right). The 30° angle results in no apparent reflected wave from the angle surface.

It must be remarked that energy is not being added during Mach reflection; the partial stagnation of the dynamic pressure between the triple point, slip line, and reflective surface is converting part of the kinetic energy into internal energy in a reduced volume, increasing the pressure loading felt by the snow slab (Needham 2010). This shock constructive interaction seems advantageous for avalanche mitigation operations since allows to enhance the charge effective range by simply using the terrain conditions.

Table 1 from ConWep summarizes the increase in overpressure obtained for different slope angles for a 9 kg TNT charge where R is the standoff distance and P_{stem} is the Mach stem pressure. The ratio between the incident shock pressure and the reflected pressure is denominated as the reflection coefficient, which for these values would be $P_{stem}/P_{s.}$

Table I. Reflection overpressure for different angles for a 9 kg TNT charge.

R [m]	P_s [kPa]	β_{slope}	P_{stem} [kPa]
1	6460	30-40	38762
2	958	30-40	4792
3	345	30-40	1379
4	179	30-40	627
5	110	35-45	331
5	76	34-55	212
6	55	35-55	143
7	45	35-60	108
8	37	30-65	81
9	31	30-75	65

According to Table I, the maximum effective range of case charges can be optimally increased by the use of the Mach reflection for certain topographical situations. The formation of this Mach stem can be achieved for a variety of slope angles. It must be mentioned that most of the theoretical and experimental data available for blast wave reflection consider an almost rigid surface. Thus, soft surfaces with different acoustic impedances are expected to influence the shock

interaction. According to Mellor (1985), the reflected pressures from snow can be about 30% lower than those from a rigid surface, but the Mach stem pressure is higher than the free-air value after Mach reflection from snow.

1.5 Standoff Distance

There is no single optimal standoff distance for an explosive yield because each blast aims to achieve a different goal. As a rule, the stronger targets will require a surface blast that leads to the highest possible overpressures near to the center of the blast (Glasstone 1977). However, because the established avalanche triggering limit is relatively low, the standoff distance may be increased to extend the effective radius. Therefore, for the purpose of inflicting widespread overpressure across the avalanche starting zone, an optimal standoff distance can be defined. Note that a blast too far from the hill does not create overpressures high enough to trigger an avalanche, but a blast too close may create local cratering and not cover the desired area.

According to the blast curves presented by Mellor (1985) for snow, the optimal standoff distance for a minimum 1 kg charge at an angle of 30-60 degrees correspond approximately to a scaled distance of 2 $m/kg^{1/3}$ (5 $ft/lb^{1/3}$). It must be noted that these curves are made on the assumption that the surface of the earth is completely unyielding and that the shock has lost no energy as a result of its interaction with surface defects such as vegetation, trees, or slope changes.

2.4 Atmospheric Scaling

The air blasts generated by the detonation of explosives charges at high elevation and cold temperatures vary 45% reduction of effectiveness from those generated at sea level or lower

altitude. In the case of 3C charges, air acts as the intermediate medium between the charge and the snow. Therefore, in order to be able to accurately predict the effectiveness of the explosive charge in delivering high pressure waves to the snow, it is important to understand how both temperature and elevation influence the interaction between the explosive shock wave and the air. The relationship of overpressure as a function of distance and time that describes the propagation of an air blast depends on the ambient atmospheric pressure, which is a function of altitude. With increasing altitude, the overpressure at a given distance will decrease, the time of arrival of the shock front will increase, and the duration of the positive phase of the blast wave will increase.

Sachs' scaling laws can be used to predict the variations in the blast wave properties with ambient conditions other than sea-level. To apply the required correction factors, the ambient temperature and pressure at the blast site must be known. For the purpose of the technical calculations, the values adopted for ambient pressure and temperature are those provided by the "U.S. Standard Atmosphere, 1976" published by the U.S. Government Printing Office, Washington, D.C. However, it should be noted that for specific blast, the calculations should be done with the actual pressure and temperature at the blast site. The correction factor for overpressure at altitude is as follows:

$$S_p = \frac{P}{P_0} \tag{1}$$

$$S_t = \left(\frac{P_0}{P}\right)^{\frac{1}{3}} \left(\frac{T_0}{T}\right)^{\frac{1}{2}} \tag{2}$$

Where S_p is the correction factor for ambient pressure, P_0 is the ambient pressure at sea level, P is the ambient pressure at altitude, S_t is the correction factor for time duration, T_0 is the ambient temperature at sea level, and T is the ambient temperature at altitude. It must be noted,

that these correction factors are valid when the target and charge location are at roughly the same altitude. If the altitude difference is less than a few thousand feet, the temperature and pressure at the mean altitude may be used. The expected accuracy of the modified Sachs scaling laws is about 20% for general applications of blast waves propagating through a real atmosphere (Needham 2010).

2. LABORATORY EXPERIMENTS

2.1 Case Charges

A total of three different case charges were built and tested at the Explosives Research Laboratory (ERL) in Idaho Springs, Colorado. Two of these were designed with a cylindrical body. One of them was built with a spherical geometry in order to compare the charge performance and the air blast produced. The casing for the cylindrical charges was made from 152.4 mm diameter PVC pipe that was 609.6 mm long and 0.5 mm thick. Every charge was composed by bulk ANFO as the main charge primed with a 454 g Pentolite booster and 30 cm of detonating cord (10.2 g/m). Figure 5 shows the geometries and orientations used during the experiments.

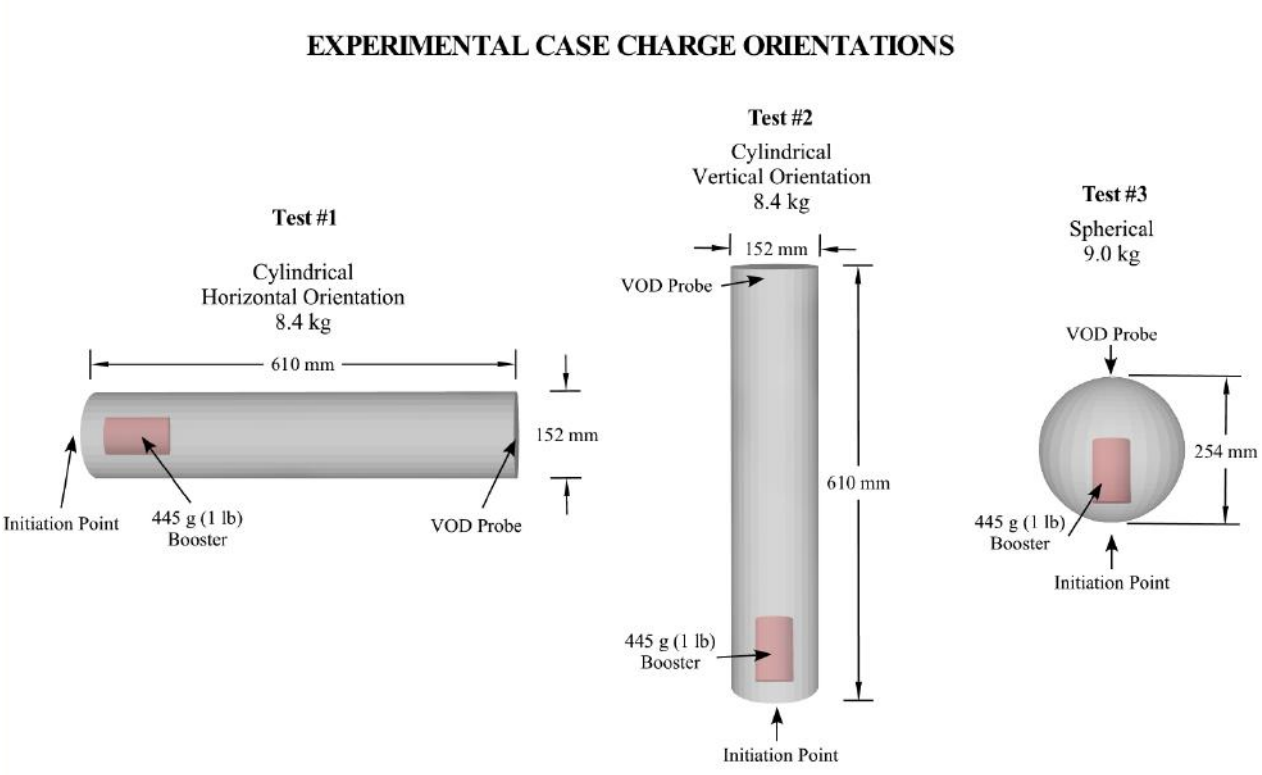

Figure 5. Experimental case charge geometries and orientations.

2.2 Experimental setup

Nine different air blast tests were conducted for evaluating the influence of the explosive charge geometry and orientation. Only three of the tests were evaluated for overpressure data while the other six evaluated the detonation velocity data from high speed imaging. The tests were conducted at the Explosives Research Laboratory (ERL) in Idaho Springs, Colorado. The atmospheric pressure and temperature were 66.8 kPa and 12.2 °C, respectively. The average elevation of the test site is 2,434 m above sea level. Tests 1 to 8 were done using cylindrical case charges while Test 9 was implemented with a spherical charge. For Test 1, the charge was placed

in horizontal position with the charge axis parallel to the ground. For Test 2, the charge was placed vertically with the axis perpendicular to the ground. The general test setup is shown in Figure 6.

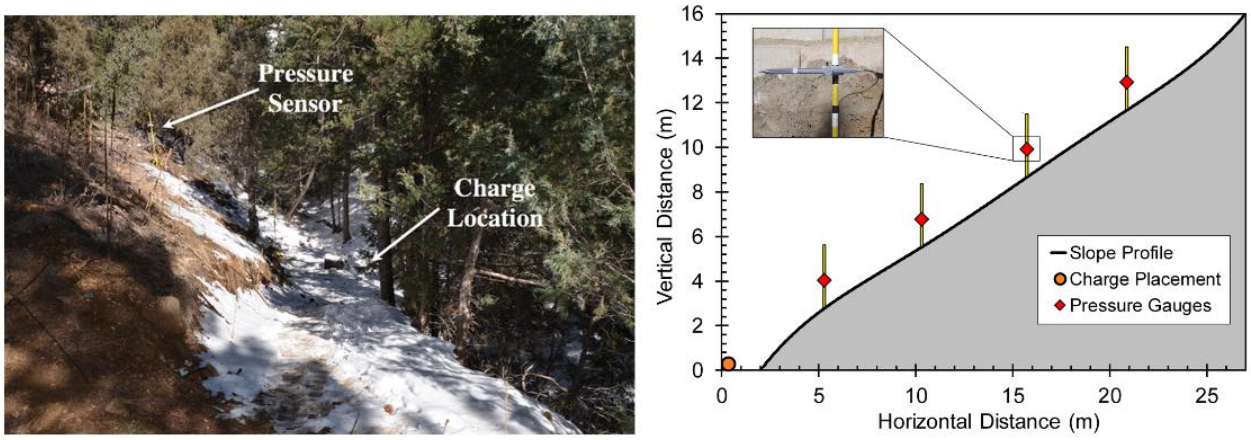

Figure 6. General test setup at the ERL (top) and slope profile of the test field and location of pressure gauges (bottom).

The test slope was profiled with a total station Topcon GTS-255 at ten different points. The total distance along the slope is 33 m with an average angle of 32 degrees. Figure 7 shows the test slope profile, and the charge and pressure sensor locations.

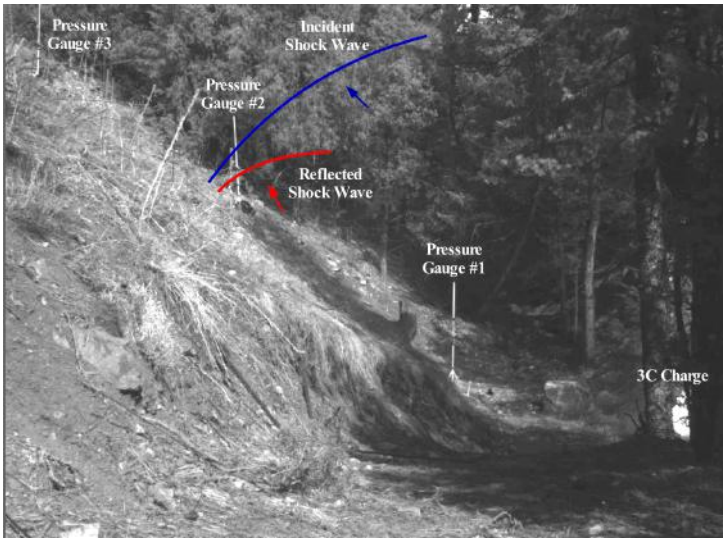

Figure 7. Slope profile of the test field and location of pressure gauges from high speed imaging camera.

The overpressure-time histories were obtained using four piezoelectric pressure transducers PCB 137A23 at four fixed locations along the slope. The gauges are located at 7 m, 12 m, 18 m, and 24 m respectively from the charge along a straight line and placed in a steel stand 1 m above the ground. The sensitivity of the sensors is 14.5 mV/kPa±15% depending on the calibration. The diaphragm was insulated using common black vinyl electrical tape to minimize thermalization of the transducer from the passing of the shock front. Additionally, the bodies of the gauges were isolated from the ground by placing vinyl electrical tape in contact with the surface of the steel stand. The four pressure sensors were connected by coaxial cables to a PCB sensor signal conditioner model 482C05 and to a Tektronix DPO3014 Oscilloscope where the signal provided by each gauge was recorded. The triggering was implemented from an EIT HB-SBS electric firing system. The signals were captured by the oscilloscope at a rate of 2.5M samples per second. Additionally, the detonation velocity was experimentally recorded using MREL

Handitrap II VOD recorder. The general performance of the cylindrical case charge was further evaluated through four additional tests where the detonation velocity was measured using the method previously described.

3. RESULTS AND DISCUSSION

3.1 ERL Test Results

As previously mentioned, the detonation performance is quantified in this paper by the detonation velocity achieved in the charge. Since the case charges tested are primarily made of ANFO, monitoring the detonation velocity becomes critical in terms of the energy output from the charges. Table II summarizes the results of the packing density and velocity of detonation obtained for the seven tests conducted.

Table II. Values of density and detonation velocity

Test	**Geometry**	**Weight ANFO**	**Density**	**VOD**
-	**-**	***kg***	***g/cc***	***m/s***
1	Cylinder	8.50	0.815	3260
2	Cylinder	8.40	0.806	3140
3	Sphere	8.60	0.865	2824
4	Cylinder	7.92	0.750	3024
5	Cylinder	8.87	0.834	3405

6	Cylinder	9.50	0.854	3294
7	Cylinder	10.11	0.908	3370

According to Table II, an average velocity of 3188 m/s was measured for the cylindrical geometry. The higher detonation velocity values are obtained for higher packing densities of the bulk explosive with a standard deviation of 208 m/s. It can be also observed that the spherical geometry shows a particularly low detonation velocity presumably due to a lower velocity value and the type of confinement. In general, the detonation appears consistent and without interruption for all tests using the cylindrical charge with a 150 mm diameter and 0.5 mm thickness.

Once the charge performance is assessed through the experimental measurements of the detonation velocity, we proceed to analyze the blast overpressure profile created by the first three tests. Figure 8 shows the raw overpressure-time record for each test with at each gauge distance. For the furthest distance, the gauge for Cylinder A failed. It can be seen that Cylinder A behaves very similar to the spherical charge in the two successful cases, albeit with a higher peak pressure. When viewing the following plots in Figure 8 it is important to not the height of the pressure spike, this will be the peak overpressure, and it is important to note the width of the pressure spike. From the time the spike occurs to the time the pressure reaches zero is the positive pulse duration or the time it take for the surrounding air to reach normal pressure. The actual time of when the spike occurs is not important as this changes for each shot and does not affect the performance of the charge.

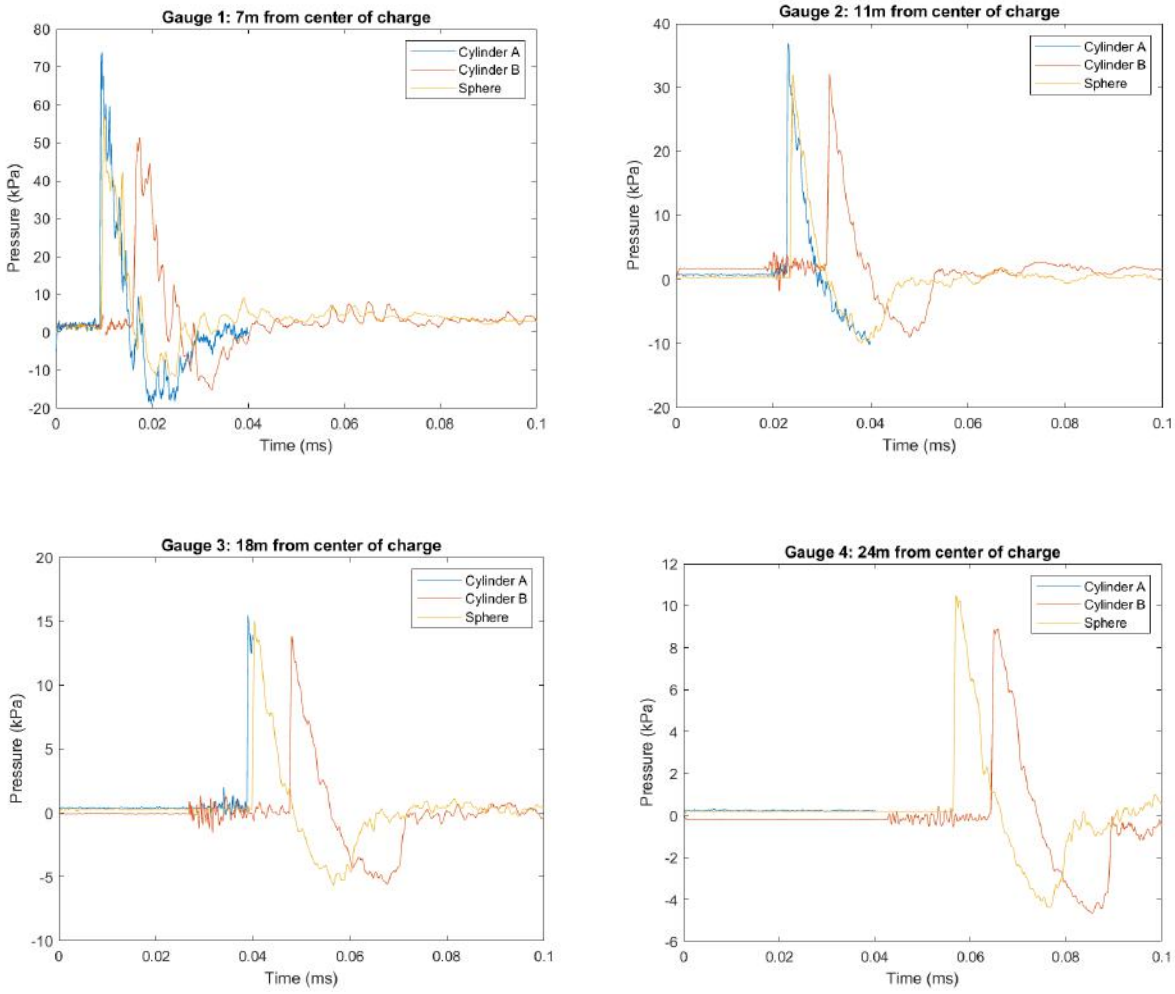

Figure 8. Overpressure-time record comparing the three charges across the four pressure gauges

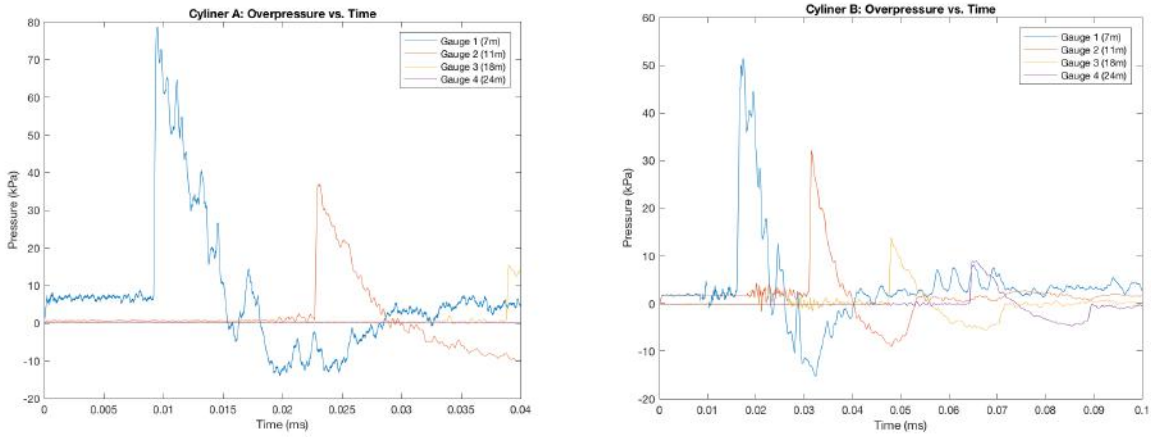

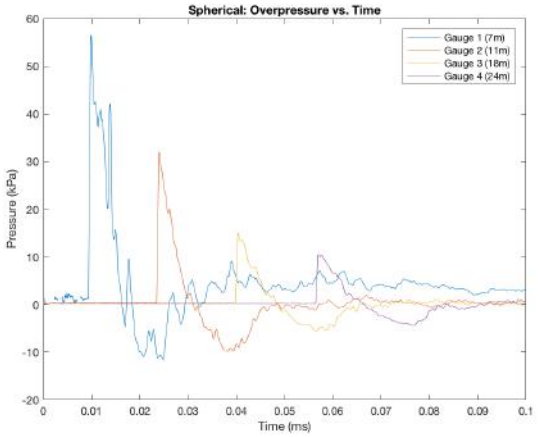

Figure 9. Overpressure vs. Time for each test, Cylinder A (Horizontal), Cylinder B (Vertical), and the Spherical charge

According to Figure 9, the peak overpressure decreases and the duration increases as one moves away from the center of the blast. Two different peaks appear at the first pressure gauge corresponding presumably to the incident blast wave and the reflected wave from the hill slope. The other three gauges only recorded a single pulse that, for the given range, it is expected to be associated to the Mach stem. In other words, the three last sensors (11 m, 18 m, and 24 m) are located after the path of the triple point.

Relating to the data analysis, it must also be taken into consideration that the maximum value recorded in the oscilloscope does not match exactly with the peak incident overpressure because of sensor overshoot (Rigby 2014). In order to obtain the actual peak overpressure, the overpressure-time record must be smoothed. This is done using the analytical methodology presented by Kinney et al. (1985) where peak overpressure, positive duration, and wave form parameter are determined and inserted into the Friedlander equation. The Kinney-Graham

equations for determining overpressure (3) and time of arrival (4) are shown below with P_{max} being the peak overpressure and t^+ being the time of arrival of the shockwave. P_a is the ambient air pressure, Z is the scaling factor for TNT equivalence, R is the distance to the charge, and W is the weight equivalent in TNT.

$$P_{max}(psi) = \frac{(808)(P_a)[1+(\frac{Z}{4.5})^2]}{\sqrt{1+(\frac{Z}{0.048})^2}\sqrt{1+(\frac{Z}{0.32})^2}\sqrt{1+(\frac{Z}{1.35})^2}} \quad (3)$$

$$t^+ = \frac{1}{c}\int_{r_c}^{r}[\frac{1}{1+\frac{6P_{max}}{7P_a}}]^{1/2} \quad (4)$$

For calculating the scaling factor which comes from experiments based off of TNT it is important to know the range of the blast, the charge weight equivalence of TNT and ambient air density at sea level (ρ_o) and ambient air density at the desired elevation (ρ). The air density is important to consider especially since these charges are used for avalanche mitigation in Colorado can be greater than 1600 m above sea level.

$$Z = \frac{(\frac{\rho}{\rho_0})*R}{W^{1/3}} \quad (5)$$

Another common analytical equation used for finding the overpressure is the Kingery-Bulmash equation, which is used in the CONWEP data presented in the following figure 10 as the red line. Polynomials are derived to find the incident shockwave overpressure, the reflected shockwave overpressure, the arrival time and the impulse duration by using least squares fitting.

Here Y is the common logarithm of the blast parameter U which is a function of a fitting constant, K, and the scaling factor, Z.

$$Y = C_0 + C_1U + C_2U^2 + C_3U^3 + \cdots + C_nU^n \tag{6}$$

$$U = K_0 + K_1T \tag{7}$$

$$C_{0,1,2,etc} = constants$$

$$K_{0,1,etc.} = constants$$

Table III summarizes the peak pressure and impulse values for each test at the four different gauge locations. Recall that the distance reported for each gauge correspond to the straight line between the sensor and the explosive charge. The gauges recorded the incident shockwave from the blast. If the gauges were to record reflected shockwave there would multiple distinct peaks for each individual gauge seen in figure 9. In addition to the multiple peaks the reflected pressure would also be higher in many cases than the incident pressure meaning these peaks would have been significantly higher than the peaks seen in figure 9.

Table III. ERL test results for different charge geometries showing peak overpressure and impulse from outdoor explosive research laboratory experiments.

Charge Weight	VOD (m/s)	Gauge 1 (7.12 m)	Gauge 2 (11.85 m)	Gauge 3 (18.15 m)	Gauge 4 (24.19 m)

Cylinder A (Horizontal)	8.5 Kg	3,291	P_s = 73.81 kPa t_p = 6 ms	P_s = 36.95 kPa t_p = 6 ms	P_s = 15.49 kPa t_p = n/a	-
Cylinder B (Vertical)	8.5 Kg	3,047	P_s = 51.45 kPa t_p = 6.9 ms	P_s = 32.13 kPa t_p = 7.5 ms	P_s = 13.83 kPa t_p = 8.6 ms	P_s = 8.90 kPa t_p = 9.8 ms
Sphere	8.6 Kg	2,708	P_s = 42.65 kPa t_p = 6.8 ms	P_s = 32.02 kPa t_p = 7.6 ms	P_s = 15.00 kPa t_p = 8.4 ms	P_s = 10.47 kPa t_p = 9.9 ms
Kinney Equation	1.8 x 6.9 Kg TNT	Pa = 66.87 kPa β=34˚s=4.5		P_s = 23.64 kPa P_t = 59.36 kPa	P_s = 11.24 kPa P_t = 24.06 kPa	P_s = 7.37 kPa P_t = 14.27 kPa

In the table above P_s is the peak overpressure and the t_p is the duration of the pulse. The positive impulse duration for the three charges did not seem to be dependent on the charge geometry. The positive impulse is the time it takes for the overpressure to reach its peak then decay back to zero. For each charge the pulse duration was calculated at all four gauge distances. However, the test for Cylinder A had some issues which did not allow the oscilloscopes to capture the data at gauge four or the entire positive pulse for gauge 3. Typically for a high explosive charge the pressure pulse should increase as distance increases from the charge, which is seen here. For cylinder B and the spherical charge, the pulse duration increases about 1 ms each successive distance increase and they reach the same magnitudes despite the difference in charge shape. The cylinder B starts at 6.9 ms pulse width at 7 m and increases to 9.8 at 24 m while the spherical charge starts at 6.8 ms at 7 m and increases to 9.9 ms at 24 m. These results show that the charge shape does not significantly affect the pulse duration. In addition to the experimental data a CONWEP simulation was done with a similar weight of ANFO that came from the values for table 1. These values reflect the experimental pressures seen in table 3 and have very similar values at

8, 11, 18, and 24m. According to the CONWEP curve the effective range to set of an avalanche where the pressure is above 3.5 kPa is up to 45 m. Also, according to this CONWEP data the reflected pressure will be able to trigger the avalanche up to 82 m, almost double that of the incident overpressure. This information shows that using the right conditions, a reflected shockwave can extend the range of the charge by double the standard distance.

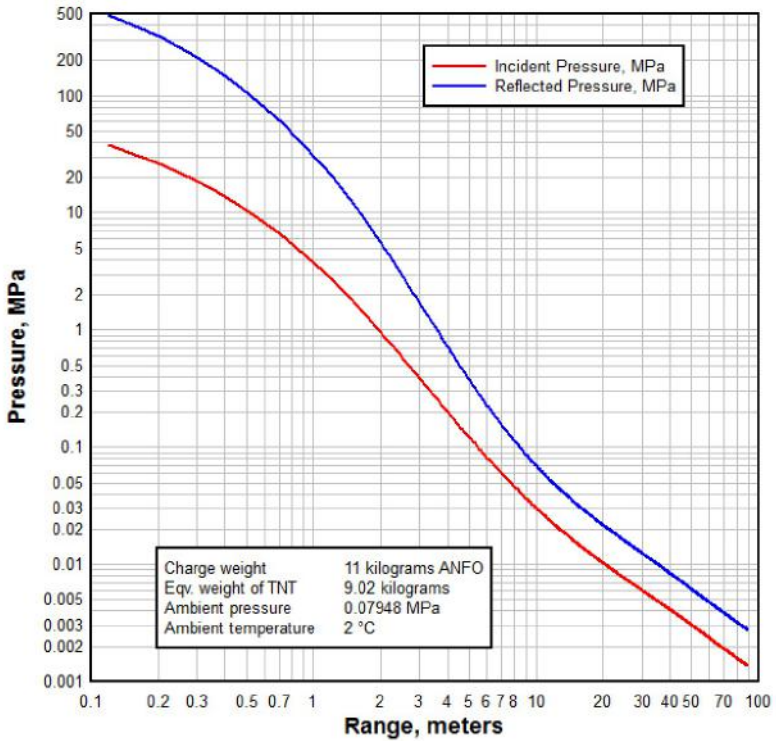

Figure 10. CONWEP data for charge weight of 11 kg of ANFO

The cylindrical charge that was detonated horizontally with the axis parallel to the ground produced almost a 30% higher overpressure at the closest pressure gauge than the vertical and spherical charges. The signal for the last gauge was lost during Test 1 due to sensor malfunction. At the third pressure gauge, the overpressures of all three charges were within 1.25 kPa of each other. This data verifies the predictive model that a cylindrical charge will produce higher

overpressures at close range, but in a far range will perform similar to a spherical charge. In order to further analyze these experimental results, the overpressure and impulse values are plotted against the results provided by ConWep for a hemispherical surface blast. ConWep calculates the blast overpressure versus range using the widely accepted Kingery and Bulmash (K-B) curves for spherical free-air TNT bursts (Kingery 1984). In this case, the software applies a correction factor for ANFO and the input atmospheric conditions:

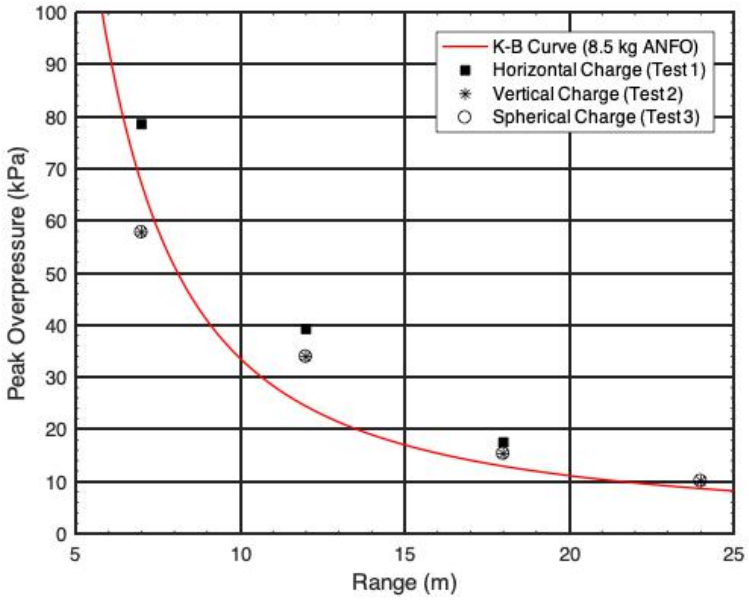

Figure 11. Overpressure plot for the three tests and the K-B curves for an 8.5 kg ANFO charge.

According to Figure 11, the last three sensors recorded experimental peak overpressure values higher than the prediction provided by the K-B curves for a hemispherical surface burst. This reveals the influence of the constructive shock wave interaction that takes place at the slope and potentially the influence of the charge geometry at close range. Figure 5 also reveals the influence of the charge geometry and orientation where the maximum output in terms of explosive-driven blast wave is obtained for the horizontal cylindrical charge. As mentioned previously it can be seen in the above figure 11 that as the pressure decays, each of the three charges start to

converge and have less of a pressure difference as the distance increases. At approximately 18 m and further, all the charges behave as an isotropic hemispherical point charge, i.e they converge with the spherical shaped charge.

3.2 CDOT Field Test Results

The results obtained from the field experiments regarding charge geometry, location, and orientation were implemented during the winter season of 2016/2017 by the avalanche mitigation crews of the Colorado Department of Transportation. Figure 12 shows a CDOT avalanche mitigation cahrge of 23 kg (50 lbs) case charge in the Vail Pass, CO. The charge is primed with two 2.3 kg (5 lbs) Pentolite boosters, safety fuse, and a number 8 detonator.

Figure 12. Image of a charge at highway bank to initiate avalanche on opposite hillside performed by CDOT in Silverton, CO.

Table IV summarizes the field test results collected by the CDOT avalanche mitigation crews during the 2017 winter season. A total of 34 shots were executed in 7 different locations in Colorado. All of them successfully triggered the avalanches with no issues reported. Table IV only shows the most relevant results for compactness.

Table IV. CDOT case charge field test results

Day	Location	No. charges	ANFO Weight per charge	Pentolite Booster	Slope Angle	Standoff distance	Effective range	Snow Depth
-	-	-	lb	lb	degrees	ft	ft	in
1/13/2017	Grand Mesa	5	40	5 (x2)	40	40	400	30
1/24/2017	Grand Mesa	7	40	5 (x2)	40	40	400	24
2/24/2017	Vail Narrows	8	50	5 (x2)	80	100	185	24
2/26/2017	LP, mm 226	1	25	5	39	5	300	10
2/26/2017	LP, Outward Bound	1	25	5	39	5	120	10
2/26/2017	LP, Big Windy	1	25	5	45	25	120	12
2/26/2017	LP, Boy Scout	1	25	5	39	25	160	6
2/26/2017	LP, No Brains	1	25	5	45	25	300	5
2/28/2017	Grand Mesa	3	40	5 (x2)	40	40	400	18
3/1/2017	LP, Outward Bound	1	25	5	39	5	100	10
3/1/2017	LP, Big Windy	1	25	5	45	25	120	12
3/1/2017	LP, Boy Scout	1	25	5	39	25	130	6
3/1/2017	LP, No Brains	1	25	5	39	25	40	5
3/1/2017	Vail Narrows	8	50	5 (x2)	80	100	185	18
3/23/2017	Grand Mesa	5	40	5 (x2)	40	40	400	60

4/4/2017	Grand Mesa	5	40	5 (x2)	40	40	400	48
12/17/2017	Grand Mesa	5	40	5 (x2)	40	40	400	30

According to the results shown in Table IV, case charges from 10 kg (25 lbs) 23 kg (50 lbs) to are able to trigger snow avalanches for a wide variety of snow depths along the different locations in Colorado. Some locations like Grand Mesa, require the use of several charges in parallel due to the length of the potential avalanche zone along the road. Different standoff distances are also reported for each location with similar charges. This is because the standoff distance is usually restricted to the road width. The CDOT avalanche mitigation crews have adopted this new case charge technique in numerous avalanche locations along the Rocky Mountains roads.

4. CONCLUSIONS

A new avalanche mitigation method was introduced using a high explosive charge placed at the avalanche runout zone. This new avalanche mitigation technique is well-suited to mountain roads presenting several advantages over the existing methods: minimum deployment time, low cost, reduced probability of misfires, and reduce operation time in the avalanche danger zone. The research work presented in this paper was done through ERL laboratory experiments where the detonation velocity and the blast physical properties are measured. Finally, field test results collected by CDOT avalanche mitigation crews during the 2017 winter season were presented

resulting in successful blasts that corresponded closely with results obtained at ERL. The new data allowed for the field tests to reach higher avalanche starting points and wider run out zones.

Because of its low cost, high availability, and safe handling, ANFO was selected as the explosive of choice for comprising the main charge in case charge designs. Alternative explosive materials such as emulsions may serve as well as viable option. Several parameters influence the final performance and energy output from highly non-ideal explosives such as ANFO, e.g., charge mass, diameter, geometry, density, external confinement, etc. Taking into consideration these factors impose several conditions on the final case charge design. The charges are proposed to have an external cylindrical shape with a minimum length/diameter (L/D) of 4, the minimum inner diameter of 150 mm, and 0.5 mm thick Polyvinylchloride (PVC) as inert confiner material. The charges must be initiated by one side and primed with the proper booster depending on the charge size.

The maximum effective range of case charges was increased by the use of the Mach reflection for certain topographical situations. The formation of this Mach stem can be achieved for a variety of slope angles. The experimental value of the peak overpressure and impulse were higher for the three charges tested than the prediction provided by the K-B curves for a hemispherical surface burst. This reveals the influence of the constructive shock wave interaction that takes place at the slope and potentially the influence of the charge geometry at close range. The experimental data showed the effective range for an 8.5 kg charge, regardless of geometry to be further than 24m, with a overpressure of about 8-10 kPa at 24m and a needed 3.5 kPa to trigger an avalanche, this shows that at 24m there three times the need pressure to trigger the avalanche. Taking the Mach reflection into account could increase this distance even further. For example, in table 1 the pressure at 7 m for the TNT charge was a similar value as the case charge in this study

and had a Mach stem pressure that is two times higher than the incident pressure. This double in overpressure will increase the range of the charge several meters past where the incident pressure could reach. In addition, the influence of the charge geometry and orientation were observed with a maximum output in terms of explosive-driven blast wave achieved for the horizontal cylindrical charge. For the current test conditions, at distances of 18-20 m, all responses from the charges converged to behave as an isotropic hemispheric point charge.

From the laboratory studies, the charge geometry, location, and orientation were implemented during the winter season of 2017 by the avalanche mitigation crews of the Colorado Department of Transportation. A total of 34 shots were executed in 7 different locations in Colorado. All of them successfully triggered the avalanches with no issues reported. The CDOT avalanche mitigation crews have adopted the new case charge as the preferred technique in numerous avalanche locations along the Rocky Mountains roads.

ACKNOWLEDGEMENTS

We would like to thank the Colorado Department of Transportation (CDOT) for funding this research project, Dr. Ethan Green for his support and for providing the field test results, and especially Tyler Weldon, David Reeves, James Walker, and Kyle Lester. We would also like to acknowledge the support of the Colorado School of Mines Mining Engineering Department for the use of the Explosives Research Laboratory in Idaho Springs as well as the AXPRO team members, Bob Lynch, Ray Johnson, Shane Robinson and Erika Nieczkoski. Lastly, we thank the students from the Explosives Engineering (Spring 2016) class that assisted in collecting the experimental data; Keith Moody, Jessica Weyand, Christian Peterson, and David Harper.

REFERENCES

British Columbia Ministry of Transportation, *EXPLOSIVE USE OPERATIONAL PLAN*, OHS 21.85 Firm No. 4000-175.

Cooper, P.W. (1996) *Explosives Engineering*. Wiley-VCH, New York.

Esparza, E.D. (1992) Spherical Equivalency of Cylindrical Charges in Free-Air. *Proceedings of 25th Explosives Safety Seminar*, pp. 403-428.

Glasstone, S. & Dolan, P.J. (1979) *The Effects of Nuclear Weapons*. United States Department of Defense and the Energy Research and Development Administration, Chapter III, Air Blast Phenomena in Air and Surface Bursts.

Kingery, C. N. & Bulmash, G. (1984) *Air blast parameters from TNT spherical air burst and hemispherical burst*. Report ARBRL-TR-02555, Army Ballistic Research Laboratory, Aberdeen Proving Ground, MD.

Kinney, G.F., Graham, K.J. (1985) *Explosive Shocks in Air*. Springer, New York.

Livingood,L.,Kanzler, J.,Elkins,J. (1990) The use of large explosive charges for avalanche hazard reduction, *International Snow Science Workshope (ISSW)* October 9-13, Big Fork, Montana, Proceedings, page 192-197

Mellor, M. (1973). Controlled release of avalanches by explosives. *Symposium on Advances in Avalanche Technology*, Reno, NV. US Forest Service Technical Report RM-3, pp. 37–49.

Mellor, M. (1985) *Blasting and Blast Effects in Cold Regions*. Part I: Air Blast, US Army Corps of Engineers, Special Report 85-25.

Miller, D.A., Tichota, R.G., Adams, E.E. (2011) An explicit model for the study of snow's response to explosive air blast, *Cold Regions Science and Technology* 69.

Needham, C.E. (2010) *Blast Waves*. Springer, Berlin.

Petes, J.,Miller,R.,McMullan,F.,*User's guid and history of ANFO as a Nuclear weapons effect simulation explosives ,* Technical Report Contract No.DNA-TR-82-156,

Petr, V. Lozano, E. (2016) CDOT Case Charge for Avalanche Control, *Technical Report for Colorado Department of Transportation.*

Rigby, S.E., Tyas, A., Fay, S. D., Clarke, S. D., Warren, J. A. (2014) Validation of semi-empirical blast pressure predictions for far field explosions – is there inherent variability in blast wave parameters. *Proceedings of 6th International Conference on Protection of Structures against Hazards*, pp. 16-17.

Short, M., Quirk, J. J., Kiyanda, C. B., Jackson, S. I., Briggs, M. E., & Shinas, M. A. (2010). *Simulation of detonation of ammonium nitrate fuel oil mixture confined by aluminum: edge angles for DSD* (No. LA-UR-10-01904; LA-UR-10-1904). Los Alamos National Laboratory (LANL).

U.S. Standard Atmosphere, 1976 National Oceanic and Atmospheric Administration, National Aeronatic and Space Administration and United State Air Force, Washington October 1976